SUPPORTING INFORMATION

Experimental part: Magnetically Induced birefringence measurements

During experiment the sample was held between poles of iron-core electromagnet (up to 2T) in a glass cell of path lengths ranging from 5mm to 130mm depending on the magnitude of the birefringence induced. The light from He–Ne laser (Zeiss) (λ= 632.8nm) was used as a probe passing through a high quality Glan–Thompson polariser (P) whose transmission axis was oriented at 45° azimuth angle with respect to the electric field direction. After turning the magnetic field on, the sample becomes birefringent with a composition-dependent time constant. As a result, the linear polarization of incident light beam passing the sample changes into the eliptical one. The quarter-wave plate (λ/4), whose optical axis is oriented along the azimuth angle of polarizer P, changes polarization from elliptical to linear with simultaneous rotation of the plane of polarisation by an angle α. The light is then passed through another linear polarizer, working as analyser (A), and reaches the photomultiplier detector. The angle α is found from the position of analyser for which light intensity is minimum. The instrument allows the precise measurement of the angle of rotation of the light polarization plane, ($\Delta\alpha$=±0.001°), which is proportional to the sample birefringence, Δn:

$$\alpha = \frac{\pi L}{\lambda}\Delta n \,. \qquad \text{(eq. S1)}$$

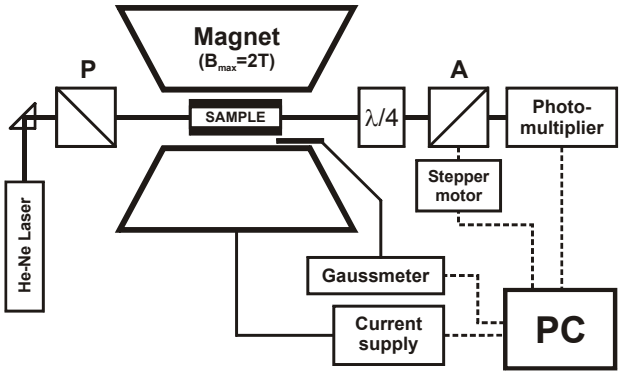

scheme 1: Polarimeter for magnetically induced optical birefringence measurements. P, A and λ/4 stays for Polarizer, Analyser and quarter-waveplate, respectively.

Optical birefringence in the liquid system always occurs as a result of preferential orientation of anisotropic molecules. This orientation may be achieved by application of any external physical fields (electric, magnetic, shear ...) [26]. In the case of magnetically induced birefringence, orientation of molecules appear because of the interaction between magnetic field and the molecular magnetic dipole moment. Here the torque is acting on the molecule trying to minimize the angle

between the directions of the field and of the dipole moment. For any molecule, also for those which do not possess the permanent dipole moment (as it is for both DBP and BEEA), the dipole moment can always be induced by the field itself. Its magnitude depends on the tensor property called the magnetic susceptibility (polarizability). If the susceptibility is isotropic, then the direction of the induced dipole coincide with the direction of the field. Because for this case the angle between the dipole and the field is zero, no torque will be acting on such molecule and no induced orientation will be observed. For this to happen the anisotropy of the susceptibility is required. This means that, in molecular coordination system, the value of susceptibility in two perpendicular directions are different. Only then the direction of the induced magnetic dipole will be different then the direction of the magnetic field that inducing it. Now the molecule will be forced to orient its direction of highest magnetic susceptibility along the magnetic field. In order to generate optical anisotropy of the whole sample by the preferential orientation of its molecules it is also mandatory that molecules are further optically (electrically) anisotropic. Just then the optical properties (refractive index) of the system in the direction parallel to the field will be different from that in the perpendicular direction, which is the definition of the birefringence. The sign of the induced birefringence (negative or positive) depends on the relative orientations of magnetic and electric susceptibility (polarizability) ellipsoids. By convention, if the direction of the highest magnetic polarizability coincides with direction of highest electric polarizability, then the induced birefringence is positive.

<u>experimental part: Pulsed field gradient spin-echo (PFG-SE) method</u>

Pulsed field gradient spin-echo (PFG-SE) method, first proposed by Stejskal and Tanner [5] and recently employed to study surfactant-based liquid mixtures [6], consists of a Hahn-Echo pulse sequence ($\pi/2-\tau-\pi$) with two identical magnetic field gradient pulses, the first applied between the 90° and 180° rf pulse (during the dephasing) and the second after the 180° rf pulse (during the rephasing) but before the echo. Following the usual notation, the magnetic field pulses have magnitude g, duration δ, and time delay Δ. The attenuation of the echo amplitude is represented by the Stejskal-Tanner equation:

$$A(g) = \exp[-\gamma^2 g^2 D_t \delta^2(\Delta - (\delta/3)] \qquad \text{(eq. S2)}$$

where D_t is the self-diffusion coefficient and γ is the nuclear gyromagnetic ratio. Note that the exponent in the equation is proportional to the mean-squared displacement of the molecules over an effective time scale ($\Delta - (\delta/3)$). For the investigated samples, the experimental parameters, Δ and δ, ranged between 20-25 ms and 1-4 ms, respectively. The gradient amplitude, g, varied from 10 to 850 G cm^{-1}.

FT-IR analysis

The analysis of this absorption thus allows to investigate the state of the alkyl chains endings. It must be noted that terminal CH_3 groups are present in both molecules, so the band is not a specific probe of one molecule or the other, but rather it is the overall result of both (composition weighted) contributions. The band is shown in Fig. S1 for all the studied compositions. It can be seen that the band shape is different in pure DBP with respect to the pure BEEA: in the former it looks more structured showing a shoulder on the high-frequency side, whereas in the latter it looks a rather sharp single peak. For all these arguments we did not consider as physically meaningful the band position so we did not take into account for it. Instead, in order to envisage any kind of structural rearrangement in the mixtures, we compared each single spectrum with that calculated by a linear, composition weighted, combination of the two pure components. The results are shown in Fig. S2: it can be seen that small deviations takes place especially in the high energy side of the band. More interestingly, such deviations tend to increase with increasing X in the range $0<X<0.5$, but tend to decrease at higher X values. This means that in the mixtures, at $X>0.5$ both DBP and BEEA absorbers tend to experiment the chemical environment characteristic of their pure state,

This behaviour confirms what observed for the P-O-H combination band and specifically that increasing association takes place when BEEA is added to DBP but when the values of $X=0.5$ is overcome, another regime is entered where the further added BEEA tends to self- segregate to form a BEEA solvent in which DBP-rich micelles float.

This fact can be seen as a further hint of nano-segregation.

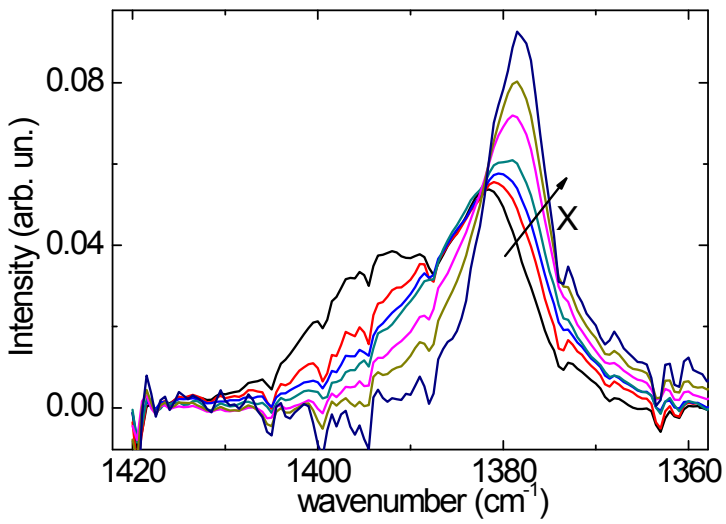

Fig. S1: FT-IR spectra in the 1420-1360 cm^{-1} range at 20°C for all the studied compositions.

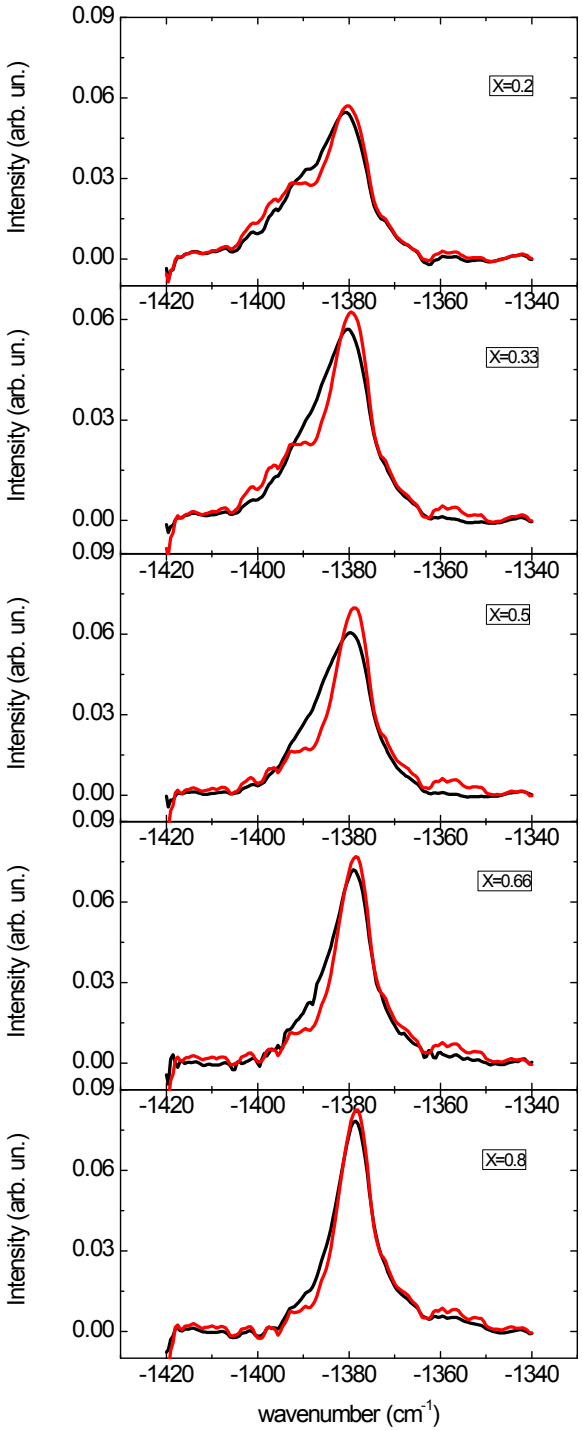

Fig. S2 comparison of each single spectrum with that calculated by a linear, composition weighted, combination of the two pure components

This aspect can be interestingly compared with those derived by the analysis of the 3000-2800 cm^{-1} spectral range, which are reported separately in the various panels of fig. S3. In this region the

peaks are due to the symmetric and antisymmetric stretching of CH_2 and CH_3 groups, as indicated in the figure (lower panel). Taking into account that these groups are located along the alkyl chain forming the cone-shaped hydrophobic portion of the surfactant molecules the relative intensity ratio of such peaks should be sensitive to the molecular lateral packing of the alkyl chains.

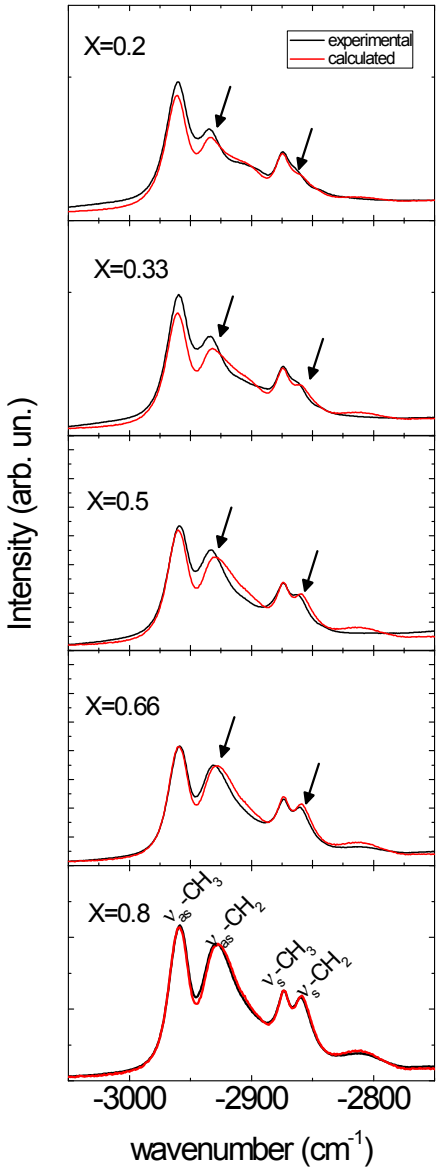

Fig. S3. Comparison between the spectra of the mixtures with the spectra theoretically calculated by a linear composition weighted combination of the spectra of the two pure components. The arrows point the peaks showing differences between the two situations.

Interestingly here we found that spectra of the mixtures are not the mere combination of the spectra of the two pure components. In fig. S3 we compare the spectrum of each mixture (each panel for

each composition) with the theoretical spectrum calculated from the spectra of the two pure components and weighted by their volume fraction, according to the pertinent composition, in the same procedure adopted for the analysis of the CH_3 umbrella bending above discussed. It can be seen, here again, that some deviation takes place, well above from the statistical error, and that the most evident differences affects the peaks due to the symmetric and antisymmetric stretching of the CH_2. In the figure, for clarity sake, the arrows point the peaks showing the most prominent differences between the two situations.

The symmetric and anti-symmetric stretching of the CH_3 are, instead, less affected by differences, especially in the peak position. This is the result of the fact that a change in the lateral packing of the alkyl chains affects more the skeletal CH_2 groups rather than the terminal CH_3 groups. The fact that the terminal CH_3 groups show less differences can be due to partial interdigitation of the alkyl chains: in this situation the terminal CH_3 groups must experience always the same chemical environment and be less sensitive than the CH_2.

This of course means that also the lateral packing somehow reflects the composition-dependent structural rearrangements driven by polar-polar interactions. Moreover, and more interestingly, it must be noted that the differences are at maximum at X=0.5 whereas at X=0.8 the experimental spectrum almost coincides with the theoretical one calculated from the linear combination of the two pure components. This confirms what observed from the POH combination band and the CH_3 umbrella bending and is another hint for the occurrence of nanosegregation at this composition.

NMR

The Arrhenius analysis of the diffusion data is reported in Fig. S4. Here, the best fit of the ln D_t vs. 1/T plot allows the determination of both the activation energy (E_A) and pre-exponential factor (A) for the diffusional process. The linear trend in the Arrhenius plots assured the validity of the two-well potential model. E_A is the energy required for the diffusion to take place, giving an information related to the local structure; A is instead associated to the molecular frequency of oscillation within each potential well. The trend of both E_A and A reflects what has been observed for the D_t values.

As it can be seen the values of E_A for DBP and BEEA are the same in the $0<X<0.5$ range and are different in the $0.5<X<1$ one. The same holds for the pre-exponential factor.

These results are in full agreement with the previous discussion concerning the self-aggregation of DBP when $X>0.5$, at which corresponds the higher activation energy respect to the BEEA, whereas, when $X<0.5$, these species form associates hetero-adducts DBP-BEEA, whose diffusional motions require more energy as the aggregates size increases.

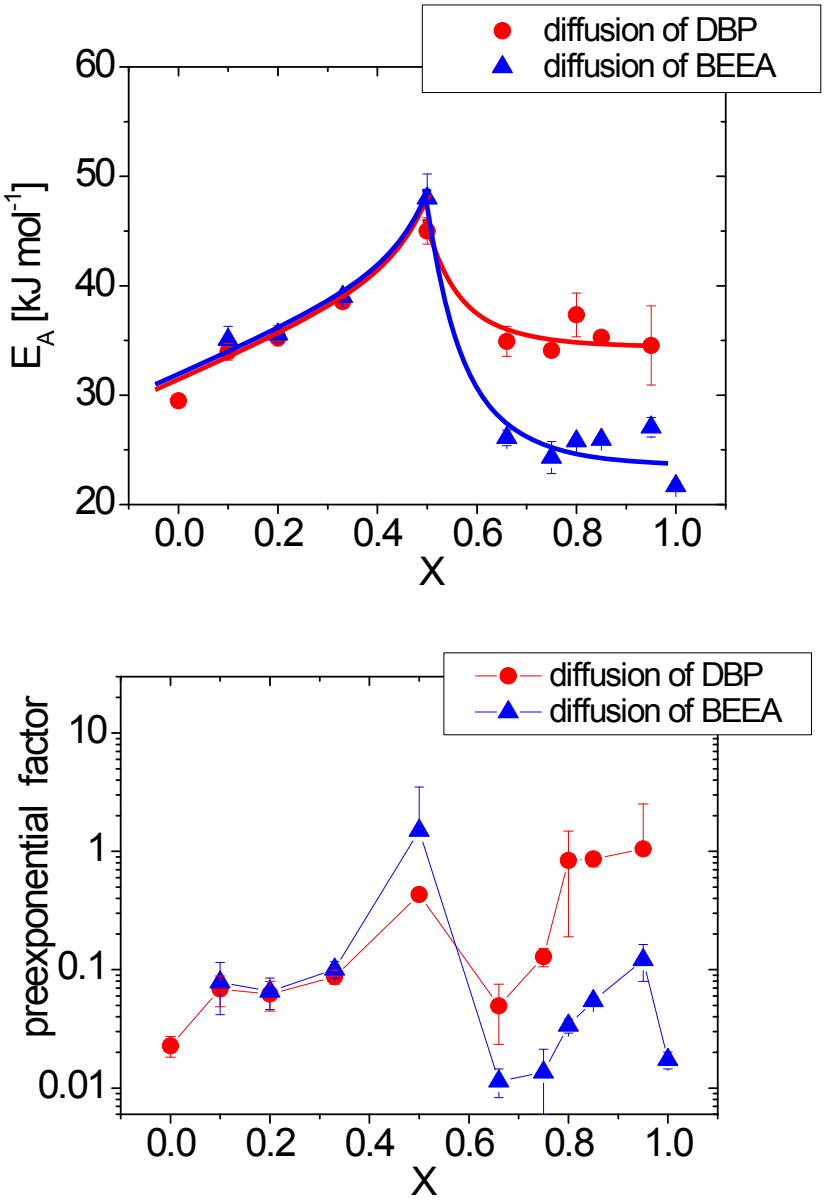

Fig. S4: Arrhenius analysis of the diffusion coefficients.

Rheology

For the rheological study we have first analysed the flow curve: i.e. the plot of the apparent viscosity as a function of shear rate for each sample and for each temperature.

In Fig. S5 it is reported a representative curve of a typically Newtonian sample (X=0, T=20°C) as compared to the sample at X=0.5 at the same temperature.

It can be observed that for the more structured sample (X=0.5) an apparent lowering of the viscosity takes place with increasing shear rate. This is the so-called shear thinning effect and is an indication of the existence, within the mixures, of soft structures which are deformed/disrupted under shear

To better quantify this effect we calculated, as indicators, the following parameters: (i) the γ_c , i.e. the value of gamma at which a deviation from constant value of viscosity is observed and (ii) the A value, i.e. the steepness with which the viscosity decreases with the shear rate derived as the slope of a quadratic function fitting the experimental data beyond γ_c). See S5 for the graphical meaning of such parameters.

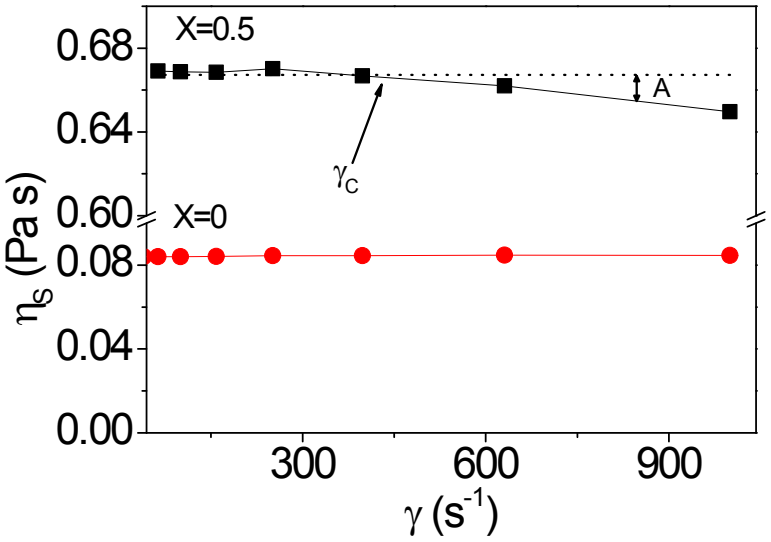

Fig. S5 Flow curves of two representative samples at 20°C. For the sample at X=0.33 the graphical meaning of γ_C and A discussed in the text is shown.

Table S1: shear thinning parameter: γ_c i.e. (the value of gamma at which a deviation from constant value of viscosity is observed), and A (i.e. the steepness with which the viscosity decreases with the shear rate)

Thinning γ_c /A		
temp	**X=0.33**	**X=0.5**
10	398/0.06	367/0.11
20	630/0.04	397/0.076
30	815/0.016	500/0.05
40		733/0.039
50		792/0.028
60		
70		

It is interesting to note that some samples (X=0.33 and X=0.5) show a slight shear thinning: in Table S1 we report the values of γ_c and A. It is evident that, as expected, the shear thinning is more evident at lower temperatures where the temperature disordering effect is less marked. This highlights the soft-interactions driven formation of aggregates which tends to a maximum at the stoichiometric composition (DBP-BEEA acid-base adducts, in accordance with the IR data.

Model to fit rheological data:

The zero shear viscosity η_S can be described by the Maxwell equation

$$\eta_S = G\tau \qquad \text{(S3)}$$

where G is the shear modulus and τ the relaxation time of the dynamic network.

According to models describing the network dynamics [13,14] these quantities scale with the volume fraction (ϕ) of the network building blocks

$$G \propto \phi^{2.25} \qquad \text{(S4)}$$

and

$$\tau \propto \phi^{x} \qquad \text{(S5)}$$

where the value of *x* is determined by the processes governing the structural relaxation time of the network. [17]

Combining these equations, a power law dependence of the viscosity from the volume fraction of the building blocks can be predicted.

In particular, similarly to concentrated solutions of rod-like micelles or polymers, [15, 16] we have found that the viscosity can be well described in terms of power laws of the type

$$\eta_S \propto \phi_V^B \qquad \text{(S6)}$$

where ϕ_V is the volume fraction of BEEA in the range 0≤X≤0.5 and the volume fraction of DBP in the range 0.5≤X≤1. The fitting parameters are collected in Table 1 in the text.

Brillouin experiments: Physical principles at the base of the technique and further considerations

Brillouin spectroscopy is an inelastic light scattering technique used to examine properties of thermally activated propagating fluctuations in condensed matter materials. In liquid and soft matter systems the method is used to sample collective molecular behavior responsible for mechanical (acoustical) wave propagation (longitudinal phonons). The basic principle of this method is that the frequency of light is being Doppler-shifted as a result of scattering onto the density wave which

travels through the system with the speed of sound. This appears as side bands (Brillouin lines) in the spectrum of scattered radiation. In any condensed matter system, the broad spectrum of thermally activated vibrational modes (phonons) exist which differ in frequency and whose dimensions ranges from atomic to macroscopic scales. Acoustic fluctuation of specific wavelength is selected in experiment by particular scattering geometry. Then the Bragg condition connects the experimental scattering angle, θ, and wavelength of probing light, λ, with the exchanged wave vector of the fluctuation by $q=4\pi n\sin(\theta/2)/\lambda$.

In order to parameterize the changes in Brillouin lineshape, the registered spectra are usually fitted using the convolution of the experimental elastic scattering profile with the expression derived on the basis of generalized hydrodynamics [19, 20]

$$I_{VV}(\omega) = A_C \frac{\Gamma_C q^2}{\omega^2 + \left(\Gamma_C q^2\right)^2} + A_B \left[\frac{\Gamma_B q^2}{\left(\omega+\omega_B\right)^2 + \left(\Gamma_B q^2\right)^2} + \frac{\Gamma_B q^2}{\left(\omega-\omega_B\right)^2 + \left(\Gamma_B q^2\right)^2} \right]$$
$$+ A_B \frac{k^2}{\omega_B} \left[A_C\Gamma_C + A_B\Gamma_B \right] \left[\frac{\omega+\omega_B}{\left(\omega+\omega_B\right)^2 + \left(\Gamma_B q^2\right)^2} - \frac{\omega-\omega_B}{\left(\omega-\omega_B\right)^2 + \left(\Gamma_B q^2\right)^2} \right] \qquad \text{(S7)}$$

The first unshifted lorentzian contribution accounts for thermal relaxations occurring on a time scale of the order of $(\Gamma_C q^2/2\pi)^{-1}$, the second term within square brackets describes the Brillouin doublet with Half-Width at Half- Maximum (HWHM) $\Gamma_B q^2$ and symmetrically shifted at the frequencies $\pm\omega_B=\pm v_B q$ while the last two terms ensures for the preservation of the first moment sum rule.

The amplitude of the scattering wave-vector translate into the spatial dimension of the acoustic fluctuation given by the sound wave-length, $\Lambda=2\pi/q$. In our experiments, conducted in back-scattering condition, with λ=532nm, $\Lambda\cong$200nm. This means that registered acoustic wave carries information about mechanical properties of the medium averaged over this spatial-scale. Any structures smaller then Λ would participate to the average and will not be seen as individual species. As in most of moderately viscous liquids, also in pure DBP and BEEA, the structural relaxation time reaches value of an order of few ps. This means that the relaxation process may effectively couple with the propagating density fluctuations (whose frequencies are of the order of few GHz) and viscoelastic behavior will be manifested. At room temperature, however, the rate of the structural reorganization of pure DBP and BEEA is high in comparison with the frequency of the hypersound. In this case the system is able to adapt to new conditions provided by the pressure wave. Doing this it loses energy mostly by the viscous flow. When DBP and BEEA are mixed, the mutual DBP-BEEA interactions give rise to the growth of local hetero-structures whose average

mobility decreases. When the relaxation process slows down, its rate will eventually equals to the rate of sound wave. If this condition occurs the phonon-structure coupling is the most efficient and the maximum in absorption is observed (see point at X around 0.75 in the discussion, but also, even at a minor extent at X=0.33). Eventually, if further change of composition makes the structural relaxation time even slower, the structure is not able to relax to new equilibrium during the period of perturbation and energy dissipation is not related to static-shear viscosity. As a result the hypersound attenuation decreases to eventually find a minimum (see point at X=0.5 in the discussion), where the structural relaxation is the slowest.